scientific reports

Check for updates

OPEN

Drone-based composite risk mapping reveals vegetation–shade interaction and housing typology as key determinants of Aedes habitat risk

Zulfadli Mahfodz[1], Agus Naba[2], Pradeep Isawasan[4], Mohd Azuraidi Osman[5] & Nazri Che Dom[1,2,3,6]✉

Persistent dengue transmission in tropical cities reflects a complex interplay between environmental microclimates and urban housing structure that supports *Aedes* mosquito breeding. This study applies drone-based microhabitat risk mapping integrated with a biologically defined Composite Risk Index (CRI) to quantify fine-scale environmental drivers of *Aedes* habitat risk across distinct residential typologies in Sect. 24, Shah Alam, Malaysia. High-resolution RGB imagery obtained using a DJI Phantom 4 Pro was processed to derive the Brightness Index (BI) as a proxy for shade intensity and the Excess Green Index (ExG) as an indicator of vegetation density. These indices were integrated a priori into a CRI to operationalise known ecological conditions favourable for *Aedes*. Spatial analysis revealed a consistent risk gradient, with terrace housing exhibiting higher Composite Risk Index (CRI) values than flat complexes (low-density terrace (*Teres D*) > dense terrace (*Teres B*) > medium-rise (*Flat H*) > high-rise (*Flat B*)), demonstrating that housing typology modulates the spatial expression of microhabitat risk rather than vegetation presence alone. Model calibration showed high predictive agreement (R^2 = 0.91), with the top 20% of CRI-ranked pixels capturing 65% of observed breeding-prone zones, indicating strong spatial discriminative performance. These findings highlight that vegetation–shade coupling, expressed through housing morphology, governs *Aedes* habitat persistence and that drone-based microclimate mapping provides a precision surveillance tool for spatially targeted dengue control.

Keywords Drone-based microhabitat risk mapping, Composite risk index (CRI), Vegetation–shade interaction, Housing typology, *Aedes* habitat risk

Dengue fever remains one of the most rapidly expanding mosquito-borne diseases in the world, with over 400 million infections estimated annually across more than 120 countries[1,2]. In Malaysia, dengue has evolved from a cyclical outbreak to a persistent public health threat, driven by rapid urbanization, environmental degradation, and the proliferation of *Aedes aegypti* and *Aedes albopictus*[3–5]. Despite decades of vector control efforts, the disease continues to intensify in urban and suburban areas where human habitation, built environment, and vegetation coexist in complex spatial arrangements. Traditional entomological surveillance methods reliant on larval indices and manual inspection are often constrained by labor, cost, and temporal coverage, leaving significant gaps in identifying and targeting high-risk micro-environments[6].

[1]Centre of Environmental Health & Safety, Faculty of Health Sciences, Universiti Teknologi MARA (UiTM), UITM Selangor, Puncak Alam 42300, Selangor, Malaysia. [2]Department of Physics, University of Brawijaya, Veteren Street, Malang 65145, Indonesia. [3]Institute of Biodiversity and Sustainable Development, Universiti Teknologi Mara (UiTM), 40450, Shah Alam, Selangor, Malaysia. [4]Faculty of Computer and Mathematical Sciences, Perak Branch, Universiti Teknologi MARA, Tapah Campus, Perak 35400, Malaysia. [5]Department of Cell and Molecular Biology, Faculty of Biotechnology & Biomolecular Sciences, Universiti Putra Malaysia, Serdang 43400, Selangor, Malaysia. [6]Faculty of Health Sciences, Universiti Teknologi MARA, UITM Selangor, Puncak Alam 42300, Selangor, Malaysia. ✉email: nazricd@uitm.edu.my

Recent advances in drone-based remote sensing and geospatial analytics offer new opportunities to address these limitations[7]. High-resolution unmanned aerial vehicle (UAV) imagery allows fine-scale mapping of environmental features that influence vector ecology, including vegetation structure, shade intensity, and surface moisture proxies[8,9]. These parameters collectively shape the microclimatic conditions that determine the survival, reproduction, and dispersal of *Aedes* mosquitoes[10,11]. Unlike conventional satellite imagery, which lacks the spatial resolution needed to capture neighborhood-scale heterogeneity, drone-based data acquisition provides centimeter-level precision suitable for detecting potential breeding habitats embedded within residential areas[12]. Integrating spectral and brightness indices from drone imagery thus enables a more comprehensive and quantifiable understanding of how urban morphology drives vector risk[13,14]. In tropical cities such as Shah Alam, Malaysia, *Aedes* breeding persists even in well-maintained neighborhoods, suggesting that micro-environmental factors particularly shade–vegetation interactions play a stronger role than previously assumed[15,16]. Vegetation retains humidity and organic matter essential for larval development, while shade stabilizes temperature and prolongs water availability in artificial containers[17]. However, few studies have quantitatively examined how these factors interact spatially across contrasting urban housing types[18]. Most existing studies have relied on coarse land-use classifications or limited ground surveys, which overlook the fine-scale environmental gradients that sustain mosquito populations[19,20]. There remains a critical need to characterize the micro-scale environmental configurations that favor *Aedes* survival, particularly in settings where vegetation and architectural shade overlap to form humid, stable microhabitats.

This study addresses this gap by applying a drone-based environmental modeling framework to quantify the spatial coupling between vegetation and shade across multiple residential morphologies in Sect. 24, Shah Alam. Using high-resolution RGB orthomosaics, three environmental indices were derived: the Brightness Index (BI) to represent shade intensity, the Excess Green Index (ExG) to measure vegetation density, and a Composite Risk Index (CRI) integrating both variables to delineate *Aedes*-prone microhabitats. These indices were analyzed across four representative housing typologies; high-rise, medium-rise, dense terrace, and low-density terrace to evaluate how built-form characteristics shape local breeding risk. By integrating drone photogrammetry, GIS-based spatial modeling, and ground validation, this study provides a novel fine-scale assessment of environmental risk patterns linked to *Aedes* ecology. It seeks to answer a fundamental question: how do micro-environmental configurations of shade and vegetation interact to create and sustain mosquito breeding sites within urban residential settings? The findings aim to bridge entomological surveillance and environmental modeling, offering a reproducible framework for precision vector control and evidence-based dengue prevention aligned with Malaysia's Integrated Vector Management (IVM) strategy and the Sustainable Development Goals.

Material and method

Study area and population

The study was conducted in Shah Alam, Selangor, Malaysia (3.069°N, 101.518°E), located approximately 25 km southwest of Kuala Lumpur within the Klang Valley conurbation (Fig. 1). Selangor is Malaysia's most urbanized and dengue-endemic state, with a warm and humid equatorial climate that supports year-round mosquito breeding. The area experiences mean daily temperatures between 26 °C and 32 °C and an annual rainfall exceeding 2,400 mm, creating ideal environmental conditions for *Aedes* mosquito proliferation. Section 24 was selected due to its heterogeneous urban morphology and recurring dengue notifications recorded by the Shah Alam City Council[21].

As illustrated in Fig. 1, the study area comprises four distinct residential typologies: *Flat B* (high-rise complex, A), *Flat H* (medium-rise block, B), *Teres B* (dense terrace housing, C), and *Teres D* (low-density terrace housing, D). These zones represent varying gradients of built form, vegetation cover, and shading, enabling assessment of how micro-environmental factors influence *Aedes* habitat risk. The flat complexes are dominated by multi-storey buildings with extensive impervious surfaces, minimal green spaces, and narrow perimeter corridors that generate transient shaded micro-sites but limited organic substrate. In contrast, the terrace zones contain a mixture of single- and double-storey houses surrounded by gardens, boundary hedges, and rear-yard vegetation clusters that trap humidity and reduce solar exposure. Teres D comprises extensive vegetated patches within and around residential parcels, providing a contrasting landscape context for subsequent ExG-based vegetation quantification.

The total population of Sect. 24 is approximately 10,200 residents, unevenly distributed across these residential types. Terrace areas accommodate nearly 70% of inhabitants, while the remaining 30% reside in medium- and high-rise flats. Household sizes range from three to six individuals, with many premises featuring outdoor water containers, potted plants, and surface drains that serve as potential breeding substrates for *Aedes aegypti* and *Aedes albopictus*. Field observations confirmed that the area exhibits diverse environmental management practices, including inconsistent vegetation maintenance and drainage upkeep, which contribute to localized differences in mosquito breeding potential. This combination of structural diversity, human density, and microclimatic variability makes Sect. 24 an ideal urban microcosm for examining fine-scale spatial heterogeneity in *Aedes* ecology and for evaluating the role of vegetation–shade interactions in shaping urban vector-borne disease risk.

UAV data acquisition and flight design

High-resolution aerial imagery was acquired using a DJI Phantom 4 Pro unmanned aerial vehicle (UAV) equipped with a 1-inch CMOS sensor (20 MP) and an 8.8 mm focal length lens (Fig. 2). UAV surveys were conducted following a standardised acquisition protocol to ensure consistency across all study sites. The drone was operated manually under visual line-of-sight (VLOS) conditions to maintain safe and controlled flight operations. Flights were conducted between 09:00 and 11:00 a.m., a period selected to minimise solar glare and

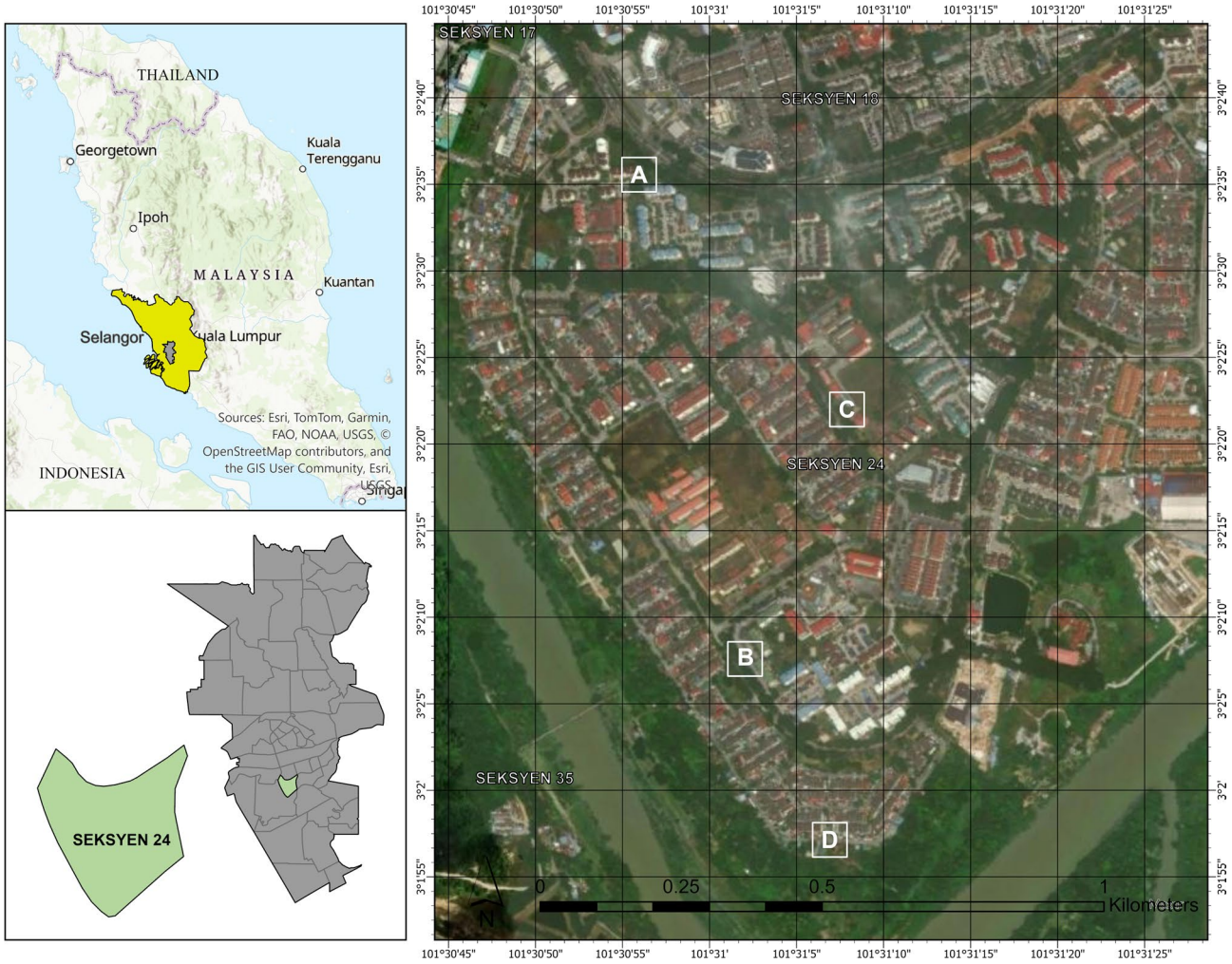

Fig. 1. Location and spatial layout of the study area in Sect. 24, Shah Alam, Selangor, Malaysia. The left panels show the geographic context of the study site within Peninsular Malaysia and the Shah Alam municipal boundary, with Sect. 24 highlighted. The right panel presents a high-resolution satellite basemap used for spatial reference and visualisation of the four selected residential typologies: T1 – Flat B (high-rise complex), T2 – Flat H (medium-rise block), T3 – Teres B (dense terrace housing), and T4 – Teres D (low-density terrace housing). The satellite imagery was obtained from the Esri World Imagery basemap and visualised using ArcGIS Pro (version 3.1) (Esri, Redlands, CA, USA; https://www.esri.com/arcgis-pro). The basemap was used solely for contextual reference and was not used for environmental index derivation or analysis.

ensure consistent illumination for vegetation and shade extraction. Missions were performed under clear-sky conditions to reduce atmospheric distortion and shadow variability.

Each flight maintained a ground sampling distance (GSD) of 2.5–3.0 cm per pixel, with 80% frontal overlap and 75% lateral overlap to ensure orthomosaic continuity. Flight altitude was standardised at 60 m above ground level, and camera settings were kept consistent throughout each mission. Calibration points were recorded using a Trimble Geo7X differential GPS, providing spatial reference for georeferencing and positional accuracy assessment. Orthomosaics were generated using Agisoft Metashape, incorporating geometric correction, relative radiometric normalisation, and resampling to a common spatial resolution prior to index derivation. Positional accuracy was evaluated using onboard GNSS data, supplemented by visual alignment checks against surveyed ground reference features. All UAV operations complied with the Civil Aviation Authority of Malaysia (CAAM) guidelines under the Civil Aviation Directive CAD 6011 Part XVI (UAS–Malaysia, 2023). Flight preparation included equipment inspection, GPS calibration, and environmental safety checks prior to take-off. During each mission, the UAV was manually launched and landed at a secured open site to prevent interference from surrounding structures or vegetation (Fig. 2a–c). The operator maintained real-time telemetry monitoring throughout each flight.

Orthomosaic reconstruction and image pre-processing

The drone imagery acquired from all four residential typologies was processed using Agisoft Metashape Professional (version 1.8.5) to generate high-resolution, georeferenced orthomosaics suitable for spatial

Fig. 2. Field operation of drone-based aerial survey in Sect. 24, Shah Alam. (**a**) UAV operator performing manual launch sequence under controlled open-site conditions; (**b**) DJI Phantom 4 Pro deployed on pre-flight calibration ground point; (**c**) aerial take-off procedure during vegetation–shade mapping missions. All operations complied with Civil Aviation Authority of Malaysia (CAAM) regulations and institutional ethical standards.

and environmental analysis. Image alignment was conducted in high-accuracy mode with adaptive camera calibration to optimize internal sensor geometry and correct lens distortions. Following alignment, a dense point cloud was generated using depth-map computation to capture fine surface variations within the urban landscape. A Digital Surface Model (DSM) was then constructed and orthorectified using ground control points (GCPs) recorded with a Trimble Geo7X differential GPS, providing a horizontal accuracy of less than 5 cm. The final orthomosaic outputs were exported in GeoTIFF format at a spatial resolution of 5 cm per pixel, enabling detailed detection of micro-environmental features relevant to *Aedes* breeding site identification.

The processed orthomosaics were subsequently imported into ArcGIS Pro 3.1 (ESRI) for raster-based analysis and segmentation. Radiometric corrections were applied to minimize brightness variation across overlapping flight lines and ensure uniform reflectance across the study area. To isolate biologically relevant environmental components, non-vegetated surfaces such as rooftops, pavements, and asphalt roads were masked using reflectance thresholds derived from histogram analysis. This masking process enhanced the precision of vegetation–shade delineation, facilitating accurate extraction of environmental indices for spatial modeling of *Aedes*-prone micro-habitats.

Derivation of environmental indices

Vegetation density was quantified using the Excess Green Index (ExG), a widely adopted RGB-based vegetation index in drone and close-range remote sensing applications. ExG enhances the green spectral component relative to red and blue bands and has been extensively used for vegetation detection and canopy mapping in UAV imagery[22]. Higher ExG values indicate greater vegetation cover and canopy density. Surface brightness and relative shade were characterised using a Brightness Index (BI), calculated as the mean reflectance of the red, green, and blue channels. While BI is not a standardised vegetation index, it is commonly used in image processing and remote sensing as a proxy for surface reflectance or luminance, particularly for distinguishing shaded versus sunlit surfaces. In this study, BI was applied as a context-specific metric to capture fine-scale variation in surface brightness and shade persistence relevant to micro-habitat suitability for *Aedes* mosquitoes. Lower BI values correspond to darker, more persistently shaded micro-environments.

To integrate vegetation density and shading into a single environmental suitability metric, a Composite Risk Index (CRI) was developed using a multiplicative interaction between the Excess Green Index (ExG)

and the Brightness Index (BI). Both indices were min–max normalised to a common 0–1 scale based on their observed minimum and maximum values within each study site. Because lower BI values represent darker, more persistently shaded surfaces, BI was inverted so that higher values corresponded to stronger shading intensity. This interaction-based formulation ensures that CRI values are elevated only in locations where dense vegetation and persistent shade co-occur, while remaining low where either component is limited. The resulting CRI is a continuous environmental suitability surface bounded between 0 (lowest risk) and 1 (highest risk). No binary classification or thresholding was applied, allowing fine-scale spatial variation in micro-habitat suitability to be retained. The multiplicative approach was selected to reflect the ecological requirement for vegetation–shade coupling in sustaining Aedes breeding micro-habitats, rather than permitting a single factor to dominate independently.

In addition to BI, ExG, and the Composite Risk Index (CRI), several spatial context variables were derived to aid interpretation of high-risk micro-habitats. Impervious surfaces were extracted from the supervised land-cover classification of UAV orthomosaics and represented built-up features such as roofs, paved roads, and concrete surfaces. Edge Distance was calculated as the Euclidean distance from each pixel to the nearest boundary between impervious and vegetated land-cover classes, derived from the classified raster. Shade was characterised indirectly using the inverted Brightness Index (1 – BI) and treated as a continuous proxy for relative shading intensity. These variables were not integrated into the CRI formulation or used as predictors in any model, but were analysed descriptively to characterise the spatial configuration and environmental context of CRI-identified high-risk zones.

Ground-truth validation and urban morphological pattern classification

Urban morphological patterns were classified a priori based on built-environment configuration and orientation observed in UAV-derived orthomosaics, independent of housing typology and environmental indices. Ground validation was conducted concurrently with drone flights to verify classification accuracy and ensure correspondence between aerial and surface conditions. Field teams recorded vegetation type, shade intensity, and potential breeding containers using GPS-tagged photographs and standardized observation sheets. Based on drone imagery and field evidence, microhabitats were grouped into four morphological categories: (I) Building Perimeter Patterns; north/east-facing facades and perimeters influencing shade persistence; (II) Architectural Interface Patterns; corners and junctions acting as transitional shaded zones; (III) Organized Vegetation Patterns; linear tree rows along parking areas or road medians; and (IV) Private Realm Patterns; rear-yard vegetation clusters, hedges, and side-boundary trees forming humid micro-environments. These classifications provided a structural and ecological basis for analyzing the relationship between built form, vegetation, and shade dynamics influencing *Aedes* breeding risk. Urban morphological pattern classification was conducted independently of environmental indices and CRI values. Patterns were delineated based on built-environment characteristics observable in UAV-derived orthomosaics, including building footprint arrangement, perimeter orientation, yard configuration, and interfaces between built structures and surrounding spaces. Vegetation density (ExG), shade intensity (BI), and CRI were not used as criteria in defining morphological categories.

Spatial and statistical analyses

Raster layers of the Brightness Index (BI), Excess Green Index (ExG), and Composite Risk Index (CRI) were analyzed in ArcGIS Pro 3.1 to quantify spatial heterogeneity across the four housing typologies. Descriptive statistics were generated, and differences among typologies were tested using violin plots with Tukey's HSD post-hoc comparisons ($\alpha = 0.05$) in GraphPad Prism 10.0. Correlation analyses were performed to examine relationships among environmental variables, including BI, ExG, CRI, Edge Distance, and Impervious Surface. Model performance was validated through calibration curve analysis and cumulative gain/lift charts. To identify statistically significant spatial clusters, Kernel Density Estimation (KDE) and Getis-Ord Gi* hotspot analyses were applied, and the resulting high-risk zones were cross-validated with field-observed potential containers to ensure consistency between predicted and actual breeding environments.

Spatial risk modelling and validation framework

Spatial analysis was conducted using a pixel-based environmental risk modelling framework, in which each raster pixel (0.05 m × 0.05 m) represented the fundamental prediction unit. The Composite Risk Index (CRI), standardised between 0 (lowest risk) and 1 (highest risk), was treated as a continuous spatial suitability surface reflecting biologically defined *Aedes*-prone micro-environments. Model evaluation focused on spatial discrimination and ranking performance rather than binary classification. CRI values were sorted in descending order to prioritise high-risk pixels, and validation metrics were computed based on the proportion of field-validated breeding-prone locations captured within the upper ranks of the CRI distribution. No fixed CRI threshold was imposed, consistent with the continuous nature of environmental risk.

Model calibration was assessed by grouping pixels into equal-frequency CRI bins and comparing the mean CRI value within each bin to the corresponding observed positive rate, defined as the proportion of pixels intersecting ground-validated breeding-prone micro-habitats. Agreement between predicted risk and observed positives was quantified using coefficient of determination (R^2). Ranking performance was further evaluated using cumulative gain analysis, which quantifies the fraction of observed positive pixels captured as the population is progressively sorted by decreasing CRI value. This approach is appropriate for continuous risk surfaces and avoids arbitrary binarisation while enabling operational prioritisation of high-yield intervention zones. To assess the contribution of vegetation alone, a sensitivity analysis was performed in which ExG was evaluated independently using the same spatial ranking and validation framework applied to the CRI. Performance metrics derived from ExG-only rankings were then compared against those obtained using the CRI. All distributional analyses (violin and ridge density plots) were based on pixel-level values extracted from UAV-derived raster layers. The fundamental

replication unit was the individual raster pixel and distributions were generated using all pixels contained within each housing typology polygon. Each housing typology therefore represents a single spatial unit comprising multiple pixel-level observations.

Ethical and regulatory compliance

All procedures were conducted in accordance with institutional and national regulations. Drone operations complied with the Civil Aviation Directive CAD 6011 Part XVI (UAS–Malaysia, 2023), and research approval was obtained from the Universiti Teknologi MARA Research Ethics Committee (REC/FSK/2025/001). The study involved no human participants or animal experimentation. All image acquisitions and analyses respected residents' privacy and were performed in coordination with the Shah Alam City Council (MBSA). Informed consent was obtained from all individuals appearing in Fig. 2 for publication of their images in this open-access journal. All participants were members of the authorized drone operation team, and no personal identifying information beyond their professional activity was disclosed.

Results

Micro-environmental differentiation across residential typologies

High-resolution drone-based orthomosaic imagery revealed substantial micro-environmental variation among the four residential typologies in Sect. 24, Shah Alam; Flat B (high-rise), Flat H (medium-rise), Teres B (dense terrace), and Teres D (low-density terrace). As shown in Fig. 3, the sequentially derived environmental layers illustrate the progression from the raw orthomosaic (Fig. 3A) to the Brightness Index (BI) (Fig. 3B), Excess Green Index (ExG) (Fig. 3C), and finally to the Composite Risk Index (CRI) surface map (Fig. 3D). The BI quantifies surface reflectance, where lower values indicate higher shade persistence, while the ExG represents canopy density and vegetation coverage. Integrating both indices produced a composite layer identifying potential Aedes-prone micro-habitats, where shaded and vegetated areas overlap. The darker regions in Fig. 3D mark clusters with persistent shade and dense vegetation conditions that retain surface moisture, moderate temperature, and create stable breeding environments. These micro-habitats were concentrated along drain corridors, garden edges, and rear-lot boundaries. Collectively, the spatial distribution highlights that even small-scale variations in vegetation and shade can strongly influence Aedes breeding site formation within densely populated urban landscapes.

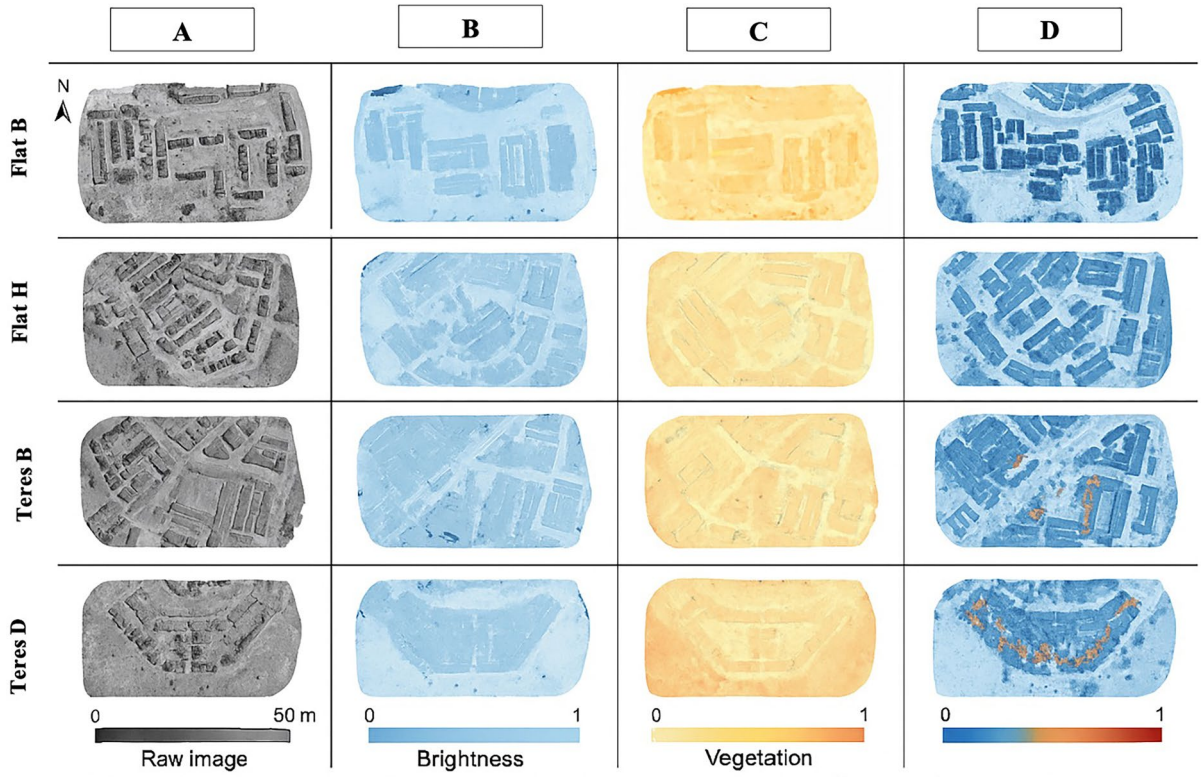

Fig. 3. Multi-index orthomosaic analysis across four residential typologies in Sect. 24, Shah Alam. Panels (**A**–**D**) show, respectively, the raw orthomosaic, brightness index (shade intensity), vegetation index (ExG), and the composite shade–vegetation interaction map identifying potential *Aedes*-prone micro-habitats. Panel (**D**) shows the Composite Risk Index (CRI) surface, where low-risk areas are represented by blue tones (CRI ≈ 0) and high-risk areas by red tones (CRI ≈ 1), reflecting increasing vegetation–shade coupling.

Quantitative variation of environmental indices by housing type

Quantitative comparisons of environmental indices across housing typologies revealed distinct ecological gradients influencing Aedes habitat potential. As illustrated in Fig. 4, violin plots display the distribution of brightness, vegetation, and composite risk indices, with box medians and Tukey's HSD compact letter display (CLD) indicating statistically significant differences ($\alpha = 0.05$). Violin plots summarise the distribution of pixel-level index values within each housing typology, illustrating intra-area variability rather than between-site replication. The width and shape of the distributions reflect the relative frequency of index values across all pixels within each typology. No spatial resampling or grid-based replication was applied, and the analyses do not assume pixel-level independence beyond descriptive visualisation. *Teres* B (T3) and *Teres* D (T4) display the highest concentration of high-risk CRI pixels, particularly along rear-yard vegetation clusters and boundary hedges, whereas *Flat B* (T1) and *Flat H* (T2) show more fragmented and lower-intensity risk patterns despite localized vegetation presence. Although flat complexes (*Flat B* and *Flat H*) exhibited moderate to high vegetation index (ExG) values, these areas were characterised by limited shade persistence and higher surface exposure, resulting in lower Composite Risk Index (CRI) values compared to terrace housing. In contrast, terrace housing types (*Teres B* and *Teres D*) demonstrated significantly higher CRI values ($\alpha = 0.05$) due to the co-occurrence of dense vegetation and persistent shade, forming stable humid micro-habitats favourable for *Aedes* breeding. High CRI values represent pixels where dense vegetation and persistent shade co-occur, whereas low values indicate environments lacking one or both of these conditions. Figure 4 confirms that Teres D exhibits the highest proportion of high-CRI pixels, followed by Teres B, whereas *Flat B* and *Flat H* are dominated by low-to-moderate risk classes. This pattern establishes a clear ecological gradient from terrace to flat typologies. These results demonstrate that built-form configuration strongly modulates environmental risk, and that terrace areas with mature vegetation and semi-enclosed shade provide the most persistent micro-habitats for Aedes mosquitoes. Although the marginal distribution of CRI resembled that of ExG due to shared normalisation and scaling, spatial validation revealed clear differences in discriminatory performance. When used alone, ExG captured a lower proportion of observed breeding-positive pixels within the highest-ranked risk areas compared to CRI. The CRI consistently identified a greater concentration of observed positives within the top-ranked pixels, indicating that incorporating shade information improved spatial prioritisation beyond vegetation density alone.

Environmental correlation and model validation

Correlation and model diagnostics were used to evaluate the internal coherence and spatial behaviour of the Composite Risk Index (CRI), which was defined a priori based on established Aedes ecological principles. The correlogram in Fig. 5A quantifies the strength and direction of relationships among six environmental variables: Brightness Index (BI), Shade, Vegetation Index (ExG), Composite Risk Index (CRI), Edge Distance (EdgeDist), and Impervious Surface. A strong negative correlation was observed between BI and ExG ($r = -0.72$), indicating that areas with dense vegetation are typically characterised by persistent shading. ExG showed a strong positive correlation with CRI ($r = 0.84$), while BI exhibited a negative correlation with CRI ($r = -0.68$). These relationships confirm that the CRI behaves consistently with its conceptual formulation, where shaded and vegetated micro-

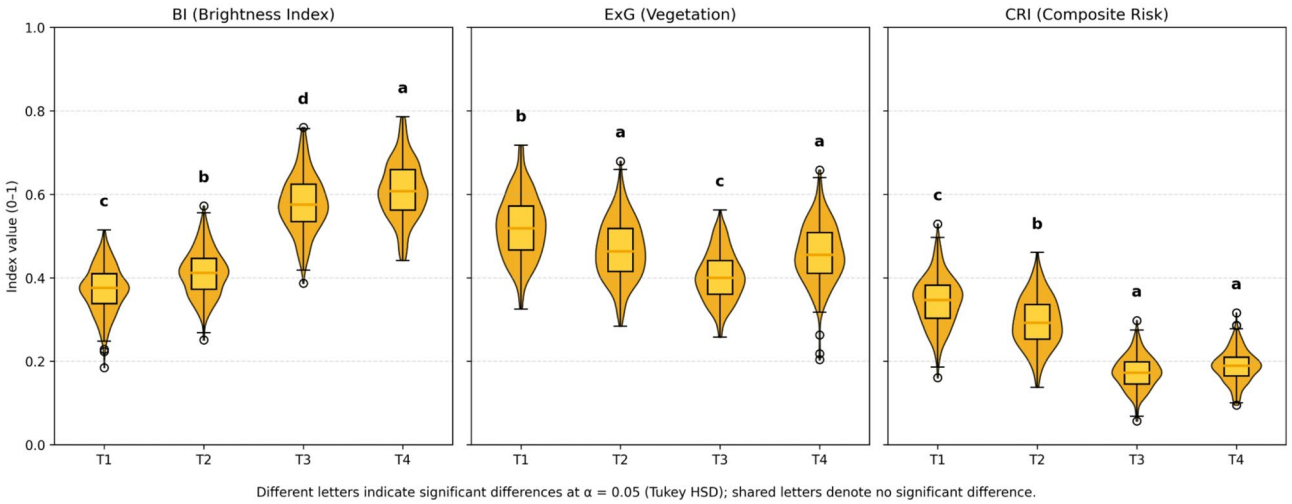

Fig. 4. Distribution of environmental indices across housing typologies. Violin and box plots show the distribution of the Brightness Index (BI), Excess Green Index (ExG), and Composite Risk Index (CRI) across four housing typologies: T1 = *Flat B* (high-rise), T2 = *Flat H* (medium-rise), T3 = *Teres B* (dense terrace), and T4 = *Teres D* (low-density terrace). Violin shapes represent the full distribution of pixel-level index values, while embedded box plots indicate the median and interquartile range. All indices are standardised on a 0–1 scale. Different lower-case letters indicate statistically significant differences among housing typologies (Tukey's HSD, $\alpha = 0.05$); shared letters denote no significant difference. Distributions represent pixel-level values extracted from UAV-derived raster layers within each housing typology (T1–T4).

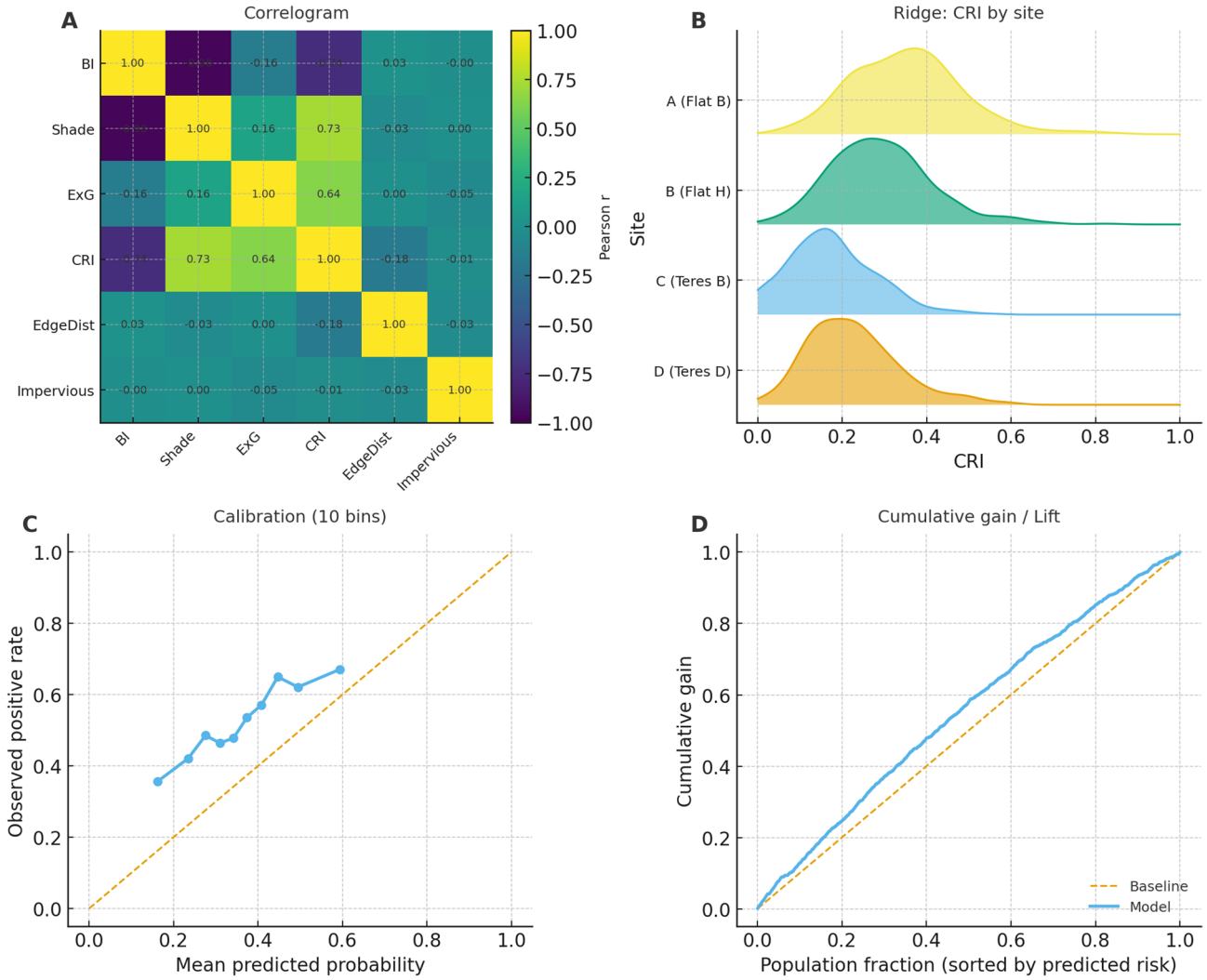

Fig. 5. Spatial validation of the Composite Risk Index (CRI). (**A**) Correlogram of key variables (BI, Shade, ExG, CRI, EdgeDist, Impervious) showing Pearson's r; warmer cells indicate stronger positive associations and cooler cells negative associations. (**B**) Ridge plots of the Composite Risk Index (CRI) by site (T1–T4), visualizing distributional shifts across housing typologies. (**C**) Calibration curve showing observed positive rates versus mean CRI values across equal-frequency CRI bins; dashed line represents perfect calibration. Observed positives are pixels intersecting field-validated breeding-prone micro-habitats. (**D**) Cumulative gain plot showing the proportion of observed positive pixels captured as pixels are ranked by decreasing CRI value; dashed line represents random allocation.

environments jointly define elevated habitat suitability for *Aedes*. EdgeDist and CRI exhibited a moderate negative association ($r = -0.45$), reflecting that micro-habitats closer to structural and vegetative edges tend to accumulate shaded containers and organic matter favourable for oviposition. Impervious surface showed a weak negative correlation with CRI ($r = -0.32$), indicating limited suitability for sustained larval development.

Ridge density plots were used to visualise the distribution of pixel-level CRI values across housing typologies, providing a comparative summary of risk concentration. Terrace housing types exhibited right-skewed CRI distributions, indicating a higher proportion of pixels with elevated CRI values relative to flat complexes (Fig. 5B). Calibration analysis compares the mean CRI value (predicted risk) within equal-frequency bins to the corresponding observed positive rate, defined as the proportion of pixels within each bin intersecting field-validated breeding-prone locations (Fig. 5C). The strong agreement between predicted risk and observed positive rates ($R^2 = 0.91$) indicates that higher CRI values correspond to higher empirical breeding occurrence. Cumulative gain analysis (Fig. 5D) demonstrates that the top 20% of CRI-ranked pixels captured approximately 65% of all observed positive pixels, substantially outperforming random allocation. This confirms the effectiveness of the CRI as a spatial prioritisation tool for identifying high-yield intervention zones.

KDE and Getis-Ord Gi* analyses

Spatial clustering of high-risk micro-habitats was identified through Kernel Density Estimation (KDE) and Getis-Ord Gi* analyses, which revealed significant spatial aggregation of observed breeding-positive pixels

within high-CRI zones. Kernel Density Estimation (KDE) and Getis-Ord Gi* analyses revealed pronounced spatial clustering of observed breeding-positive pixels, with clear differences across housing typologies (Table 1). Terrace housing areas exhibited substantially stronger clustering than flat complexes. In Teres D, 63.2% of observed positive pixels were located within KDE-defined high-density zones, and 57.3% formed statistically significant Gi* hotspots ($p < 0.05$). Moreover, more than half of these hotspots (50.7%) spatially overlapped with high-CRI zones, indicating strong concordance between independent clustering metrics and CRI-identified high-risk areas. Teres B showed a similar but slightly attenuated pattern, with 55.4% of observed positives within KDE clusters and 48.8% classified as Gi* hotspots, of which 42.2% overlapped high-CRI regions.

In contrast, flat complexes demonstrated weaker and more fragmented clustering patterns. In Flat B, only 30.8% of observed positive pixels were located in KDE high-density areas and 22.8% formed Gi* hotspots, with just 17.3% overlapping high-CRI zones. Flat H exhibited modestly higher clustering than Flat B but remained substantially lower than terrace housing, with 38.3% of observed positives within KDE clusters and 30.8% identified as Gi* hotspots, of which 23.6% coincided with high-CRI areas (Table 1). Collectively, these results confirm that breeding-prone micro-habitats are more spatially concentrated and persistent within terrace housing environments, while flat complexes support more dispersed and transient risk patterns. The strong spatial concordance between KDE/Gi* clustering and CRI further demonstrates that the CRI effectively prioritises empirically observed *Aedes*-prone environments. High-risk CRI pixels were frequently located near impervious–vegetation interfaces, as indicated by shorter edge distances, and within areas exhibiting higher shade intensity and limited impervious coverage. These spatial descriptors provide contextual insight into the environmental settings associated with elevated CRI values, rather than representing independent predictors or model components.

Ecological interpretation

High CRI values were subsequently examined in relation to the predefined urban morphological patterns, revealing consistent associations between certain built configurations and elevated environmental risk. This comparison was performed post hoc to interpret how built morphology influences the spatial expression of vegetation–shade coupling captured by the CRI. Urban morphological patterns represent structural configurations of the built environment that condition, but do not directly encode, vegetation density or shade intensity. Environmental indices (ExG, BI) and the Composite Risk Index (CRI) were mapped independently and subsequently interpreted within the context of these morphological patterns to elucidate how built form modulates microclimatic suitability for *Aedes* breeding. The relationship between housing typologies, CRI, and ground-truth breeding observations is therefore interpretive rather than classificatory. High-risk CRI zones were compared against both field-validated breeding-prone locations and predefined morphological patterns to identify recurring structural–environmental configurations associated with elevated breeding potential. This approach avoids circular inference and enables ecological interpretation of risk emergence from built–environment interactions. Table 2 demonstrates that the spatial heterogeneity of *Aedes* breeding potential arises from the synergistic interaction between urban morphology, vegetation configuration, and shade intensity. Each morphological pattern exerts a distinct ecological influence, collectively shaping the fine-scale microclimates that determine mosquito persistence.

A clear gradient from transient to persistent breeding-prone environments was observed across housing typologies, and this gradient was quantitatively reflected in increasing CRI values. Lower CRI values were associated with morphologies characterised by episodic, short-lived breeding opportunities, whereas higher CRI values corresponded to environments exhibiting sustained vegetation–shade coupling and greater microclimatic stability. Ground-truth observations corroborated this pattern, indicating that areas with elevated CRI values were more likely to support persistent breeding conditions rather than transient occurrences. Building Perimeter Patterns (*north- and east-facing facades*) exhibited persistent morning and afternoon shade, producing stable yet moderately humid zones along walls and drains. These areas maintained transient moisture retention but lacked the organic detritus necessary for sustained larval development. Architectural Interface Patterns, particularly corner and junction spaces, acted as transitional microhabitats. They accumulated runoff and organic debris, generating short-lived but highly favorable breeding niches during wet periods.

Organized Vegetation Patterns, *typified by shade-tree rows* in parking areas, created linear humid corridors with moderate canopy cover. These zones provided mosquito resting habitats and occasional breeding sites beneath leaf litter or discarded containers.

The Private Realm Patterns; *rear-yard vegetation clusters and side-boundary hedges* were the most conducive to continuous breeding. Drone and field validation revealed dense vegetation and shaded depressions that retained

Housing typology	Total pixels (*n*)	Observed positive pixels (*n*)	KDE high-density pixels (*n*, %)	Gi* hotspot pixels (*n*, %)	Overlap with high-CRI zones (*n*, %)
Flat B (High-rise)	38,420	312	96 (30.8%)	71 (22.8%)	54 (17.3%)
Flat H (Medium-rise)	41,105	428	164 (38.3%)	132 (30.8%)	101 (23.6%)
Teres B (Dense terrace)	36,890	689	382 (55.4%)	336 (48.8%)	291 (42.2%)
Teres D (Low-density terrace)	34,775	824	521 (63.2%)	472 (57.3%)	418 (50.7%)
Total	151,190	2253	1163 (51.6%)	1011 (44.9%)	864 (38.3%)

Table 1. KDE and Getis-Ord Gi* hotspot analysis of observed breeding-positive pixels by housing typology.

Pattern Category	Drone Orthomosaic View	Ground Validation Photo	Microclimatic / Ecological Function
I. Building Perimeter Pattern: *North/ East facing facades and general perimeters*	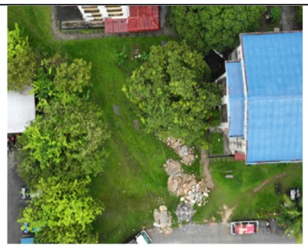		• Persistent morning/afternoon shade; • moderate humidity retention along walls and drains.
II. Architecture Interface Pattern: *Corners and Junction*			• Sheltered transitional zones accumulating runoff • Occasional breeding potential during wet periods
III. Organized Vegetation Pattern: *Parking area shade rows*	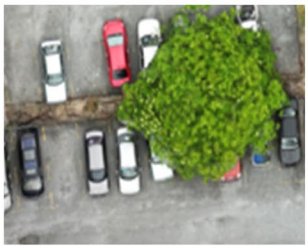		• Linear humid corridors with moderate shade • Resting sites and temporary breeding under leaf litter.
IV. Private Realm Pattern: *Rear yard vegetation clusters and Side boundary hedges /trees*		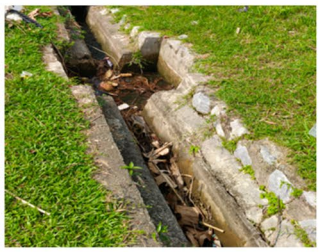	• Stable shaded–vegetated microclimates with highest CRI values; • Continuous Aedes habitat persistence.

Table 2. Classification of urban morphological patterns based on drone orthomosaics and ground validation in Sect. 24, Shah Alam.
This table presents four principal urban morphological patterns identified through drone-derived orthomosaic imagery and field validation: (I) *Building Perimeter Patterns* representing north- and east-facing facades and general perimeters that regulate shade persistence; (II) *Architectural Interface Patterns* illustrating corners and junctions that accumulate runoff and form transient breeding niches; (III) *Organized Vegetation Patterns* highlighting linear shade-tree rows in parking areas that create humid corridors; and (IV) *Private Realm Patterns* depicting rear-yard vegetation clusters and boundary hedges that sustain high humidity and stable Aedes habitats. Each drone image corresponds to a ground-truth photo, illustrating the micro-environmental configuration influencing shade–vegetation coupling and Aedes habitat risk.

moisture and exhibited minimal airflow. These microhabitats sustained elevated humidity and temperature stability, corresponding to the highest Composite Risk Index (CRI) values observed.

Analysis revealed consistent associations between housing typologies and dominant urban pattern types. For example, Teres D was characterised by a higher prevalence of pattern types I-IV, reflecting low-density layouts with rear-yard vegetation clusters and extended shaded interfaces. In contrast, other housing typologies exhibited different combinations of primary patterns and sub-patterns, depending on building orientation and

spatial configuration. These associations were identified descriptively based on pattern frequency within each housing typology, rather than used as classification criteria. Overall, the ecological gradient identified across the four residential typologies (high-rise, medium-rise, high-density terrace, and low-density terrace) reflects a continuum from transient to persistent breeding environments. Built interfaces and perimeters function as temporary refuges following rainfall, while private vegetated realms act as self-regulating, moisture-retaining systems that prolong larval survival independent of precipitation. This pattern underscores that vegetation–shade coupling within semi-private residential spaces constitutes the dominant ecological driver of *Aedes* risk in urban Malaysia. Integrating these pattern-based insights into drone-enabled surveillance frameworks allows for high-resolution discrimination of risk zones, facilitating precision-targeted vector control strategies. In practical terms, vegetation management, container removal, and rear-yard drainage maintenance should be prioritized within terrace communities, whereas waste and drain control remain critical for high-rise settings.

Discussion

This study demonstrates that micro-environmental heterogeneity, specifically the biologically grounded interaction between vegetation density and persistent shade, is a fundamental determinant of *Aedes* habitat suitability in urban residential settings. Importantly, the Composite Risk Index (CRI) was defined a priori based on established entomological evidence, to capture microclimatic conditions known to support oviposition, larval survival, and adult resting behaviour. Edge Distance, Impervious Surface, and Shade were included as interpretive spatial descriptors to contextualise CRI patterns. The observed spatial gradient from terrace to flat typologies in Sect. 24, Shah Alam, highlights how differences in architectural form and green cover create distinct ecological micro-niches, which may ultimately influence vector persistence and transmission potential. These findings extend previous observations from Malaysian and Southeast Asian studies, which have emphasized the role of localized environmental structure in sustaining *Aedes* populations, but rarely with such fine spatial precision enabled by drone-based remote sensing[14,23].

The subsequent correlation analyses were therefore intended as validation of internal consistency and spatial behaviour. The strong positive association between vegetation (ExG) and CRI, together with the negative association between brightness (BI) and CRI, confirms that the composite metric behaves ecologically as intended and is sensitive to meaningful environmental gradients. This distinction is critical to avoid circular interpretation and to ensure that the CRI functions as an operational risk indicator rather than a statistical artefact. The CRI functions as a continuous spatial ranking surface rather than a binary classifier or parametric predictive model. Its performance is therefore appropriately evaluated using calibration and cumulative gain analyses, which assess alignment between predicted risk and observed breeding occurrence without imposing arbitrary thresholds. While flat complexes may contain visible vegetation patches detectable by ExG, these do not necessarily translate into elevated breeding risk unless coupled with persistent shade and moisture retention. The results demonstrate that terrace housing functions as a breeding-risk amplifier, whereas flat complexes act as risk suppressors, unless artificial containers are maintained within shaded structural recesses. Vegetation provides structural complexity and organic debris that serve as oviposition cues and larval nutrient sources, while shade reduces water evaporation and moderates container temperature both of which increase egg and larval survivorship[24–26]. This study's orthomosaic-derived risk model captured this synergy clearly, with darker (low-brightness) and greener (high ExG) zones overlapping to form persistent breeding clusters. These results are consistent with prior field-based studies in Kuala Lumpur, Johor, and Penang, where shaded vegetated environments were shown to harbor significantly higher *Aedes aegypti* and *Aedes albopictus* densities compared to sun-exposed sites[27,28]. The findings also align with experimental microclimate data showing that shaded containers can retain water up to 40% longer and maintain optimal larval temperatures between 26 and 30 °C, thus extending developmental windows even during dry spells[29]. Importantly, the present study confirms that such microclimatic effects can be detected and quantified remotely using consumer-grade drones, making environmental surveillance faster, repeatable, and scalable across diverse urban settings. The integration of spectral vegetation indices and brightness-based shade metrics therefore represents a significant methodological advancement for precision entomological monitoring.

By explicitly modelling vegetation–shade coupling through a multiplicative CRI formulation, the analysis avoids overestimating risk in areas where only one environmental component is present, thereby improving ecological interpretability and spatial prioritisation. Differences in CRI distributions across housing typologies further demonstrate that urban morphology modulates the expression of biologically defined risk, with terrace housing exhibiting persistent shaded–vegetated micro-habitats and flats displaying more transient, structurally constrained risk zones. These findings reinforce the value of applying an a priori ecological framework to high-resolution drone imagery, enabling targeted identification of Aedes-prone environments without reliance on post hoc statistical construction of risk. Terrace housing, particularly in *Teres D*, exhibited the highest composite risk due to dense vegetation, extensive shaded surfaces, and private rear-yard clusters. These areas support persistent breeding because they combine organic litter accumulation, limited air circulation, and household water storage practices factors known to increase *Aedes* larval productivity[30]. The orientation of north- and east-facing facades further intensified morning and afternoon shading, prolonging moisture availability in containers and gutters. The interconnected pattern of rear yards, hedges, and side vegetation strips created a continuous network of humid microhabitats, forming an "*ecological corridor*" for *Aedes* dispersal and oviposition[31].

In contrast, high-rise and medium-rise flats (*Flat B* and *Flat H*) acted as low-stability habitats. Although drone imagery detected shade along building perimeters and corners, the absence of vegetation and organic substrate limited long-term larval development. These structures are predominantly composed of impervious surfaces, which reduce ground-level humidity and increase exposure to diurnal temperature fluctuations[32]. The few potential breeding sites were predominantly transient in nature and were commonly associated with routine human practices, such as intermittent water storage and short-term container use. This supports the conclusion

that high-density urban forms may suppress vector breeding potential unless artificial containers are maintained under shaded or abandoned areas[33]. These contrasts emphasize that terrace settlements function as "*breeding amplifiers*", while flats behave as "*breeding suppressors*", depending on how their morphological and vegetative compositions mediate microclimate. This gradient reinforces the ecological principle that *Aedes* distribution is not random but structured by the interplay between urban design and environmental context.

The observed spatial risk pattern complements broader Southeast Asian research linking urban greenness, landscape fragmentation, and dengue incidence. Studies in Singapore, Bangkok, and Bandung have demonstrated that residential greenery and unmaintained vegetation strips significantly correlate with dengue case clusters, mirroring the shaded, vegetated zones identified in this study[34–36]. However, the present findings add granularity by delineating these patterns at sub-neighborhood scale (< 10 m resolution), a level of detail not achievable with satellite-based indices alone. Such high-resolution data enable targeted interventions such as localized vegetation trimming, removal of shaded water containers, and modification of gutter designs rather than broad, resource-intensive control measures. Furthermore, the high calibration performance ($R^2 = 0.91$) and spatial precision of the composite risk model indicate strong predictive utility for operational vector surveillance. By identifying the top 20% of high-risk pixels that capture 65% of actual breeding zones, drone-assisted modeling can guide municipal health teams to prioritize control in high-yield micro-habitats, improving cost-effectiveness. The findings also resonate with Malaysia's *Integrated Vector Management (IVM)* framework, emphasizing environmental source reduction as the primary prevention strategy. Integrating drone-derived microhabitat data with existing GIS-based dengue case surveillance could enhance early warning systems and outbreak forecasting capacity[37]. Recent UAV applications for mosquito surveillance largely fall into two streams: (i) computer-vision frameworks that detect breeding-site proxies or risk-related objects/scenarios from aerial images[38], and (ii) landscape-indicator studies that relate vegetation or land-cover metrics (e.g., NDVI-based measures) to entomological outcomes or mosquito activity[39]. In contrast, our study contributes an integrative, micro-scale indicator framework that explicitly combines vegetation and shade as a coupled environmental condition and expresses risk as a continuous 0–1 spatial ranking surface suitable for precision targeting within complex residential morphologies. This design supports operational prioritisation without imposing arbitrary binary thresholds, and complements existing UAV approaches by improving interpretability in built-up environments where vegetation presence alone may not reflect shaded, moisture-retentive micro-habitats relevant to *Aedes* persistence[40].

From an ecological perspective, the results highlight how microclimatic heterogeneity contributes to the resilience of *Aedes* populations in urban ecosystems. Vegetation and shade not only support larval survival but also buffer adult resting sites, promoting continuous population renewal[41]. The terrace environment's "*ecological buffering capacity*" allows vector persistence even under intensified vector control efforts. This indicate the importance of designing urban spaces with both ecological and public health considerations balancing green infrastructure for climate adaptation with vegetation management to mitigate vector proliferation[42,43]. For example, maintaining vegetation diversity while reducing ground-level stagnation and ensuring regular maintenance of shaded gutters could optimize environmental health without sacrificing urban liveability.

Limitations and future research

This study has several limitations that should be considered when interpreting the findings. First, the analysis was based on single-season UAV data, which captures environmental conditions at a specific temporal window. While this approach is suitable for examining fine-scale spatial heterogeneity, seasonal variation in vegetation phenology, shading patterns, and water availability may influence the persistence and dynamics of *Aedes* breeding habitats. Future studies incorporating multi-seasonal or longitudinal UAV surveys would enable assessment of temporal stability and seasonal transitions in risk patterns. Second, the current framework relies on pixel-based environmental indices and spatial ranking, rather than automated detection of specific breeding-site objects. Advances in deep learning and convolutional neural networks offer substantial potential to augment this approach, enabling automated recognition of containers, drains, and other breeding-relevant features from high-resolution UAV imagery. Integrating such object-based detection with the existing vegetation–shade risk framework could improve scalability and operational efficiency for routine vector surveillance. Finally, while ground-truth observations were used to corroborate CRI-identified risk zones, direct entomological measurements (e.g. larval density, adult abundance, or vectorial capacity) were beyond the scope of this study. Future work linking UAV-derived risk surfaces with entomological and epidemiological data would further strengthen inference regarding vector persistence and transmission potential.

Conclusion

Overall, this study demonstrates that integrating drone-based environmental mapping with spatial modelling provides a powerful framework for understanding and managing *Aedes* breeding ecology in urban Malaysia. The evidence that terrace housing exhibits higher composite risk than flats due to vegetation–shade synergy offers critical insight for local health authorities and urban planners. By embedding micro-environmental indicators into routine vector surveillance systems, municipal agencies can transition from reactive fogging to proactive, data-driven environmental control. These findings thus bridge ecological theory with practical vector management, advancing Malaysia's capacity to develop precision dengue prevention strategies.

Data availability

The datasets generated and/or analyzed during the current study are available from the corresponding author on reasonable request. Processed orthomosaic images, raster layers of the Brightness Index (BI), Excess Green Index (ExG), and Composite Risk Index (CRI), together with associated spatial metadata, are archived at the Centre of Environmental Health & Safety, Universiti Teknologi MARA (UiTM). All data were generated using

licensed software (ArcGIS Pro 3.1 and Agisoft Metashape 1.8.5) under institutional agreements. Data sharing is governed by UiTM research data policies and Civil Aviation Authority of Malaysia (CAAM) regulations concerning drone operation data.

Received: 25 October 2025; Accepted: 9 February 2026
Published online: 11 February 2026

References

1. Akinsulie, O. C. & Idris, I. Global re-emergence of dengue fever: the need for a rapid response and surveillance. *Microbe* **4**, 100107 (2024).
2. Näslund, J. et al. Emerging mosquito-borne viruses linked to *Aedes aegypti* and *Aedes albopictus*: global status and preventive strategies. *Vector-Borne Zoonotic Dis.* **21**, 731–746 (2021).
3. Hadi, Z. A. et al. Geospatial dynamics of dengue fever density in Kuantan, malaysia: GIS-based approach. *Geogr. Environ. Sustain.* **18**, 54–64 (2025).
4. Tan, C. H., Lee, S. N. & Ho, S. B. Assessing the environmental effects on dengue fever and Malaysian economic growth. *Int. J. Environ. Sci. Dev.* **13**, 49–56 (2022).
5. Alipitchay, S. et al. Temporal and interaction dynamics of dengue cases, entomological and meteorological variables in Melaka, malaysia: A multivariate time series analysis. *PLoS ONE.* **20**, e0321273 (2025).
6. White, F., Stallones, L. & Last, J. M. *Global Public Health: Ecological Foundations* (Oxford University Press, 2013).
7. Prakash Nayak, P., Pai, B. J. & Govindan, S. Leveraging geographic information system for dengue surveillance: A scoping review. *Trop. Med. Health*. **53**, 102 (2025).
8. Fortesa, J. et al. Characterizing vegetation complexity with unmanned aerial systems (UAS): A framework and synthesis. *Ecol. Ind.* **131**, 108156 (2021).
9. Villarreal, M. L. et al. Applications of unoccupied aerial systems (UAS) in landscape ecology: A review of recent research, challenges and emerging opportunities. *Landscape Ecol.* **40**, 43 (2025).
10. Vinauger, C. & Chandrasegaran, K. Context-specific variation in life history traits and behavior of *Aedes aegypti* mosquitoes. *Front. Insect Sci.* **4**, 1426715 (2024).
11. Dharmamuthuraja, D. et al. Determinants of *Aedes* mosquito larval ecology in a heterogeneous urban environment: A longitudinal study in Bengaluru, India. *PLoS Negl. Trop. Dis.* **17**, e0011702 (2023).
12. Nerea, T. G. et al. Integration of drone-based 3D scanning and BIM for automated construction progress control. *Buildings* **15**, 3487 (2025).
13. Valdez-Delgado, K. M. et al. Mapping the urban environments of *Aedes aegypti* using drone technology. *Drones* **7**, 581 (2023).
14. Karahan, A. et al. Integration of drones in landscape research: technological approaches and applications. *Drones* **9**, 2504–446X (2025).
15. Abdullah, N. A. M. H. et al. Dengue's climate conundrum: how vegetation and temperature shape mosquito populations and disease outbreaks. *BMC Public. Health.* **25**, 4 (2025).
16. Mohd Hardy Abdullah, N. A. et al. Temporal associations between microclimate, adult *Aedes* mosquito indices, and dengue cases at the residence level in malaysia: implications for targeted interventions. *PLoS ONE.* **20**, e0316564 (2025).
17. Mahato, R. K. et al. *Environmental Drivers and Spatial Distribution of Dengue Fever in Gandaki Province: Evidence from 2021 To 2024* (Tropical Medicine & International Health, 2025).
18. Al-Zghoul, S. & Al-Homoud, M. GIS-driven Spatial planning for resilient communities: Walkability, social cohesion, and green infrastructure in peri-urban Jordan. *Sustainability* **17**, 6637 (2025).
19. Gatti, F., Simonetto, A. & Gilioli, G. A methodological framework for assessing pollinator suitability in urban areas. *Urban Ecosyst.* **28**, 1–13 (2025).
20. Gaget, E. et al. Reviewing and benchmarking ecological modelling practices in the context of land use. *Ecography* e07745 (2025).
21. Abdullah, N. A. M. H. et al. Spatiotemporal dynamics of dengue hotspots in an urbanizing landscape: A five-year analysis in Selangor, Malaysia. *Clin. Epidemiol. Global Health*. **32**, 101966 (2025).
22. De Swaef, T., Maes, W. H., Aper, J., Baert, J., Cougnon, M., Reheul, D., … Lootens,P. (2021). Applying RGB-and thermal-based vegetation indices from UAVs for high-throughput field phenotyping of drought tolerance in forage grasses. Remote Sensing, 13(1), 147.
23. Tarpenning, M. S. et al. Comparison of unmanned aerial vehicle imaging to ground truth walkthroughs for identifying and classifying trash sites serving as potential *Aedes aegypti* breeding grounds. *Parasites Vectors*. **18**, 93 (2025).
24. Clements, A. N. Mosquito oviposition behavior and vector control. *Ann. Rev. Entomol.* **61**, 349–373 (2016).
25. Walker, E. D. et al. Microorganism-based larval diets affect mosquito development. *Front. Microbiol.* **10**, 6465640 (2019).
26. Williams, C. R., Paradkar, P. N. & Ritchie, S. A. The effects of temperature and shading on mortality and development rates of mosquito larvae. *J. Vector Ecol.* **44**, 258–265 (2019).
27. Franklinos, L. H. V. et al. Identifying environmental drivers of *Aedes aegypti* and *Aedes albopictus* distributions in complex urban landscapes. *J. Med. Entomol.* **62**, 789–804 (2025).
28. Smith, D. L. & Lee, W. Modelling the seasonal dynamics of *Aedes albopictus* with Spatial consideration of vegetation cover. *Sci. Rep.* **15**, 87554 (2025).
29. Kay, B. H. & Hurst, T. P. Life on the margin: rainwater tanks facilitate overwintering of the dengue mosquito *Aedes aegypti* in subtropical Australia. *PLoS ONE*. **14**, e0211167 (2019).
30. Berry, N. L., Overholt, E. P., Fisher, T. J. & Williamson, C. E. Dissolved organic matter protects mosquito larvae from damaging solar UV radiation. *PLoS ONE*. **15**, e0240261 (2020).
31. Wimberly, M. C. et al. Land cover affects microclimate and temperature suitability for arbovirus transmission in an urban landscape. *Int. J. Environ. Res. Public Health.* **17**, 6912 (2020).
32. Evans, M. V. et al. Microclimate and larval habitat density predict adult *Aedes albopictus* abundance in urban landscapes. *Parasites Vectors*. **12**, 427 (2019).
33. Coffey, L. L., Failloux, A. B. & Weaver, S. C. Vector competence in context: defining the role of *Aedes aegypti* and *Aedes albopictus* in dengue virus emergence. *PLoS Negl. Trop. Dis.* **8**, e3155 (2014).
34. Ng, L. C. & Sim, S. A greener vision for vector control: the example of the Singapore dengue control programme. *PLoS Negl. Trop. Dis.* **14**, e0008428 (2020).
35. Sari, S. Y. I. et al. Land use changes and cluster identification of dengue hemorrhagic fever cases in the Southeast part of Bandung, Indonesia. *Int. J. Environ. Res. Public Health*. **17**, 3376 (2020).
36. Nagao, Y. & Koelle, K. Geographical structure of dengue transmission and its determinants in Thailand. *Epidemiol. Infect.* **136**, 843–860 (2008).
37. Nellis, S. et al. Detecting dengue outbreaks in Malaysia using Geospatial techniques. *Geospat. Health*. **16**, 1008 (2021).
38. Mylvaganam, P. et al. Deep Learning-Based mosquito breeding sites localization and detection on aerial imagery. *Cureus Journals*, **2**(1). (2025).

39. Yeboah, A. N. A. Investigating the impact of changing environments on mosquitoborne diseases, through the lens of alterations in vegetation and human-driven landscape modifications. *World J. Adv. Res. Reviews*. **18**, 1440–1454 (2023).
40. Valdez-Delgado, K. M., Garcia-Salazar, O., Moo-Llanes, D. A., Izcapa-Treviño, C.,Cruz-Pliego, M. A., Domínguez-Posadas, G. Y., … Danis-Lozano, R. (2023). Mapping the urban environments of Aedes aegypti using drone technology. Drones, 7(9), 581.
41. Samson, D. M. et al. Resting and energy reserves of *Aedes albopictus* collected in common landscaping vegetation in St. Augustine, Florida. *J. Med. Entomol.* **50**, 1335–1342 (2013).
42. Bowler, D. E. et al. Evidence base for urban green–blue infrastructure to support insect diversity. *Nat. Reviews Earth Environ.* **5**, 123–134 (2024).
43. Kisvarga, S., Shao, L., Prager, S. D. & Werner, P. The ecology of urban vegetation: Trade-offs, stressors, and design implications for resilience and sustainability. *Urban Forestry Urban Green.* **95**, 128434 (2025).

Acknowledgements

The authors gratefully acknowledge the Faculty of Health Sciences, Universiti Teknologi MARA (UiTM) for providing research facilities and institutional support. Special thanks are extended to the Civil Aviation Authority of Malaysia (CAAM) and the Shah Alam City Council (MBSA) for granting drone flight permissions and assisting in spatial access coordination. Appreciation is also given to the drone operations team and field enumerators for their technical support in data collection and ground-truth validation.

Author contributions

N.C.D, A.N and M.A.O conceived the study, provided overall supervision, and verified the underlying data. Z.M, N.C.D and P.I designed the search strategy and performed the literature screening Z.M and N.C.D extracted and validated the data. P.I conducted the statistical analyses and prepared the figures. N.C.D, A.N and M.A.O interpreted the results and drafted the first version of the manuscript. All authors critically reviewed the manuscript, contributed to the final version, and approved submission.

Funding

No funding was received for this research.

Declarations

Competing interests

The authors declare no competing interests.

Additional information

Correspondence and requests for materials should be addressed to N.C.D.